The Journal of Chemical Physics

Investigation of the low-energy stereodynamics in the $Ne(^3P_2) + N_2$, CO reactions

Cite as: J. Chem. Phys. **153**, 104306 (2020); https://doi.org/10.1063/5.0022053
Submitted: 16 July 2020 . Accepted: 20 August 2020 . Published Online: 14 September 2020

Junwen Zou, and Andreas Osterwalder

The Journal of Chemical Physics ARTICLE scitation.org/journal/jcp

Investigation of the low-energy stereodynamics in the $Ne(^3P_2) + N_2$, CO reactions

Cite as: J. Chem. Phys. 153, 104306 (2020); doi: 10.1063/5.0022053
Submitted: 16 July 2020 • Accepted: 20 August 2020 •
Published Online: 14 September 2020

Junwen Zou and Andreas Osterwalder[a]

AFFILIATIONS

Institute for Chemical Sciences and Engineering, Ecole Polytechnique Fédérale de Lausanne (EPFL), 1015 Lausanne, Switzerland

[a]Author to whom correspondence should be addressed: andreas.osterwalder@epfl.ch

ABSTRACT

We report on an experimental investigation of the low-energy stereodynamics of the energy transfer reactions $Ne(^3P_2) + X$, producing $Ne(^1S) + X^+$ and $[Ne–X]^+$ ($X = N_2$ or CO). Collision energies in the range 0.2 K–700 K are obtained by using the merged beam technique. Two kinds of product ions are generated by Penning and associative ionization, respectively. The intermediate product $[Ne–X]^+$ in vibrationally excited states can predissociate into bare ions (X^+). The experimental ratio of the NeX^+ and X^+ product ion yields is similar for both molecules at high collision energies but diverge at collision energies below 100 K. This difference is explained by the first excited electronic state of the product ions, which is accessible in the case of CO but lies too high in energy in the case of N_2.

I. INTRODUCTION

In recent years, there has been a rapid increase in work targeting the study of cold and ultracold chemistry under highly controlled conditions.[1–16] Many interesting physical phenomena such as orbital resonances, quantum tunneling, or reactant reorientation start to become observable only at very low collision energies.[4,6,14] Recent developments permit the use of molecular beams to study low-energy collisions, either by co-expanding reactants in molecular beams, by performing crossed beam experiments at low collision angles, or by using Stark or Zeeman deceleration and the guiding of neutral molecules.[14,16–24] One of these techniques is the merged beam approach where two supersonic expansions are superposed such that the collision energy is given only by the velocity difference of the two beams.[6,25–27] Several studies were conducted in the past years where the merged beam technique has been used to observe shape-resonances, state-dependent reactivity, and stereodynamics.[6–11]

To achieve the full control of reagents in a gas phase reaction, one would like to actively manipulate the collision energy, state distribution, and the relative orientation of the reagents. Previous stereodynamics studies were mostly conducted in crossed molecular beam experiments at collision energies above 300 K.[28–33] The first study of cold collisions with steric control was conducted on the KRb + KRb reaction in an optical lattice.[34] More recently, oriented HD was collided with D_2 in an intra-beam collisions study,[14] and magnetically oriented $Ne(^3P_2)$ was used to study the $Ne(^3P_2)$ + Ar and $Ne(^3P_2) + N_2$ reactions by the merged beam method.[9–11]

The last two of these examples are prototypical energy transfer reactions, several of which have been studied in our lab in the past years.[35] In general, colliding an internally excited metastable species A^* with other ground state reactants BC can lead to different reactions as follows:

$$A^* + BC \rightarrow A + BC^+ + e^-, \quad (1)$$

$$\rightarrow ABC^+ + e^-, \quad (2)$$

$$\rightarrow A + B + C^+ + e^-. \quad (3)$$

Reaction (1) is called Penning ionization (PI), reaction (2) is associative ionization (AI), and reaction (3) is dissociative ionization (DI). All these reactions have been studied extensively in the past decades, both theoretically and experimentally.[36–38] They are barrier-less reactions, where one of the reaction products is an ion, and they offer themselves as ideal candidates for low-energy reactivity studies.[35] Researchers in Perugia used a combination of Penning

ionization electron spectroscopy and theoretical modeling to study the reactions between Ne($^3P_{2,0}$) and rare gases Ar, Kr, and Xe, as well as molecules such as H_2O and N_2O.[39–43] In their models, all reactive channels are described by a combination of anisotropic interaction potentials and complex coupling functions that project the neutral excited state on the charged product states. This approach enabled the extraction of full stereodynamical information, angles of acceptance for different reaction channels, and the determination of orientation-dependent reactivities. An important finding was that at low-energy collisions between Ne($^3P_2$) and a rare gas atom, the ratio of the cross sections for AI and PI, σ_{AI}/σ_{PI}, is maximum for neon atoms in the $|J, \Omega\rangle = |2, 2\rangle$ entrance channel. The explanation invokes the less repulsive wall in the $V_{|2,2\rangle}$ potential, which appears at an intermediate distance of the Ne*–Rg potential curve and opens a pathway that is favorable for the trapping in the potential well of the exit channels. In contrast, at high collision energies, the branching ratio between AI and PI drops rapidly because the reactions provide ionic products confined in the repulsive region of the exit channels that lead to dissociated ions.

In our experiments, A* normally is a metastable rare gas atom, most often neon in the $^3P_2$ state. This state is paramagnetic, and a magnetic multipole guide can be used to control the direction of the beam and transport it to the reaction zone while maintaining its collimation.[25] We have found that the atoms emerging from the guide are state-selected and polarized even after the 30 cm of free-flight between the end of the guide and the collision region, and they can, thus, be oriented in a weak magnetic field.[44] The polarization of paramagnetic species in a magnetic guide has its origin in the dependence of the transmission on the magnetic quantum number m_J.[17] Only low-field seeking states are efficiently guided, meaning that only $m_J > 0$ is retained, and in Ne($^3P_2$) (henceforth labeled Ne*), the depolarization is sufficiently slow that no explicit guiding fields are required to maintain the uneven population distribution until the atoms reach the reaction zone. Because inside the guide, the field direction depends on the position within the guide, the neon atoms are not oriented despite the polarization. However, once they have left the guide, they can be oriented in an external field with a well-defined direction. At any given collision energy, the orientation of the total angular momentum vector, $\vec{J}$, of the Ne* can, thus, be manipulated. Because the direction of the relative velocity $\vec{k}$ in the merged beam experiment is fixed, rotating the direction of the external field $\vec{B}$ is equivalent to rotating Ne* relative to the incoming reactant BC. The ion yields from different ionization channels can then be probed as a function of this orientation to measure reactive cross sections σ_{AI} and σ_{PI} as a function of the magnetic quantum number m_J in the laboratory frame. In the molecular reference frame, m_J is not a good quantum number, and a transformation from the laboratory to the molecular frame is needed. Here, Hund's angular momentum coupling case (c) is used, defining the Ω quantum number as the projection of the angular momentum $\vec{J}$ on the inter-particle axis.[45–47] Reactivities can, thus, be determined as a function of Ω by expressing the known populations for states with different m_J quantum numbers in terms of Ω.

The products of AI, PI, and DI have different masses and can be easily distinguished by detecting them in a mass spectrometer, and performing these studies in the presence of a controlled magnetic field has been used in the past to demonstrate the sensitivity of the branching ratio to the field direction.[32,33] We have recently studied the Ne($^3P_2$) + Ar and Ne($^3P_2$) + N_2 reactions with orientation control of the Ne($^3P_2$) and found that the branching ratio between reactions (1) and (2) is sensitive to the external magnetic field direction at collision energies above 50 K. At lower energies, the steric effect is lost and the reactivities are the same for all directions of the magnetic field.[9–11] In contrast, the branching between reactions (1) and (3) in Ne($^3P_2$) + ND_3 is insensitive to the direction of the magnetic field over the entire energy range probed here.[48]

Associative ionization leads to a van der Waals bound charged complex $[Ne–X]^+$.[49] If X is a molecule, this complex can be formed with vibrational excitation of the molecular component. Because the binding energy of the complex is of only a few 100 cm^{-1}, in small molecules a single quantum of vibrational excitation is more energy than the van der Waals bond energy. As a consequence, internal energy redistribution leads to dissociation of the $(Ne\cdots X)^+$–bond. AI ions can, therefore, predissociate to bare X^+ ions, a process which is fast on the time scale of our experiments.[50] Thus, detected X^+ ions can originate either from PI or from AI followed by predissociation (PD). Our recent study of the Ne* + Rg (Rg = Ar, Kr, Xe) reactions demonstrate that Penning ionization is largely insensitive to the magnetic field direction.[10,51] In contrast, the formation of N_2^+ ions in the Ne* + N_2 reaction is angle-dependent.[9] We attribute this difference to the predissociation of NeN_2^+ formed by AI, leaving the PI channel angle-independent. Only after the exclusion of predissociation does the direct comparison between the cross sections for AI and for PI become possible. In the present paper, we describe our recent experiments on the Ne* + CO reaction, which is compared to the results from the Ne* + N_2 reaction. It is found that the propensity for AI is larger in CO than in N_2, an observation which we attribute to a reaction path through an electronically excited state of CO^+, while no electronically excited product states are accessible in the case of N_2^+.

II. EXPERIMENT

A detailed description of the experimental apparatus is given elsewhere.[25] Briefly, a supersonic expansion of metastable Ne(^3P_J), generated by an Even–Lavie valve with dielectric-barrier discharge (DBD),[52] is merged with a supersonic expansion of X (X = N_2, CO) by turning the beam path of Ne* onto the axis of the X beam using a 1.8 m long, curved permanent-magnet multipole guide. The guiding dynamics of metastable neon depend on the magnetic quantum number and yield a polarized Ne sample of exclusively the $^3P_2$ state because neither $^3P_0$, which is not paramagnetic, nor the short-lived $^3P_1$ reach the end of the guide. The Ne* speed is controlled by varying the valve temperature from ≈200 K–250 K, leading to center velocities between 700 m/s and 760 m/s. The molecular beam of CO or N_2 is formed by expanding a mixture of He and the respective molecule through a second Even–Lavie valve and injected tangentially into the magnetic guide. Based on the previous experiments on the same setup, the rotational temperature of the molecules is estimated to be ~20 K.[53] Molecular beam velocities of 750 m/s–1700 m/s are obtained by varying the seeding ratio with He between 1:10 and 30:1 (He:molecule), which leads, in combination with the Ne* velocities, to collision energies in the range

E_{coll}/k_B = 200 mK–700 K (k_B is the Boltzmann constant). Collision energies below ≈40 mK can be reached in principle;[10,26] however, because the distributions of longitudinal and transverse relative velocities become comparable, the experiment does not permit steric control in this regime.

Collision products, in this case X^+ and $[Ne–X]^+$ (for X = CO or N_2), from PI and AI, respectively (the DI channel is closed in these reactions), are formed in the presence of a controlled magnetic field, generated through two pairs of solenoid magnets arranged at 90°, and extracted in a home-built time-of-flight (ToF) mass spectrometer (MS). Current control on each of the magnets permits to set the direction of the magnetic field while the magnitude is kept at 10 mT. In the present experiments, the relative velocity vector $\vec{k}$ always points along the beam direction.

Inside the guide, states of Ne^* with different magnetic quantum numbers m_J experience different transverse forces, resulting in different transmissions through the guide.[17] The actual populations for the different m_J states have been determined spectroscopically, and they do not depend on the magnetic field applied during the experiment.[44] The populations p_{m_J} for different m_J states were obtained by performing REMPI spectroscopy with different laser polarizations and have been determined to be $p_0 = 0.087 \pm 0.015$, $p_1 = 0.75 \pm 0.02$, and $p_2 = 0.163 \pm 0.025$.[11]

These populations, together with the selected angle θ_{kB} between $\vec{B}$ and $\vec{k}$, are used to calculate populations in the molecular reference frame, as a function of Ω. This analogy with Hund's case (c) implicitly treats X as an atom also for the cases studied here. This is justified by the assumed long Ne–X distances during reactions and the fact that some rotational states are populated that turn X into an effectively isotropic object.

Wigner D-matrices are used, for each magnetic field orientation, to determine the Ω specific populations, p_Ω, from the measured p_{m_J},

$$p_\Omega(\theta_{kB}) = \sum_0^J p_{m_J} w_q |d^J_{\Omega,q}(\theta_{kB})|^2, \quad (4)$$

where θ_{kB} is the angle between the relative velocity, k, and the magnetic field direction, B, the w_q are weighting coefficients that are, respectively, 2 and 1 for Ω = 1, 2 and Ω = 0.[11,45] For each of the reaction channels, the total ion yield is then proportional to the cross sections for the different Ω substrates and is given as

$$I_{AI,PI} \propto \sum_{\Omega=0,1,2} p_\Omega(\theta_{kB}) \sigma^{AI,PI}. \quad (5)$$

III. RESULTS AND DISCUSSION

Sample experimental data obtained for the Ne^* + CO reaction are shown in Fig. 1. Panel (a) shows an example of the mass spectrum, recorded at a collision energy E_{coll}/k_B of 352 K and one particular orientation of the magnetic field, θ_{kB} = 90°. The red and blue peaks show CO^+ and $Ne–CO^+$ ions, respectively. The gray peak is residual H_2O, and the rest is background (BG). Each such time-of-flight profile is obtained by counting product ions from some thousand molecular beam pulses. The integration of ion signals and

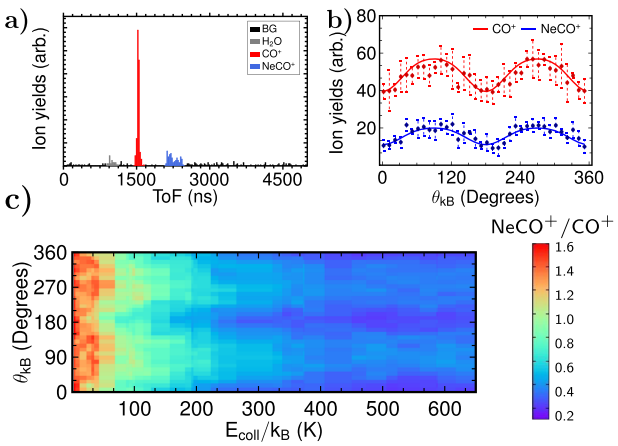

FIG. 1. (a) Time-of-flight spectrum at a collision energy of 352 K and θ_{kB} = 90° for the Ne^* + CO reaction. (b) Experimental ion yields as a function of θ_{kB} in the molecular frame. (c) Two-dimensional plot of the $NeCO^+/CO^+$ ratio for the range of angles and collision energies.

measuring them as a function of the magnetic field direction, θ_{kB}, produces curves like the one shown in panel (b) for the same collision energy. Multiple mass spectra are recorded at each angle, yielding statistical distributions that are the basis of the error bars (one standard deviation). Finally, the complete dataset for CO is shown in Fig. 1(c) as the angle- and energy-dependent ion yield ratio $r(\theta_{kB})$ (termed reactivity here) between the CO^+ and $Ne–CO^+$ yields. Analyzing the reactivity rather than the raw ion signals eliminates most of the noise and signal fluctuations.

Figure 2 shows angle-dependent ion yields for Ne^* + CO [panels (a) and (b)] and Ne^* + N_2 [panels (c) and (d)] at different collision energies. Panels (a) and (c) show results obtained at a collision energy of 600 mK; and panels (b) and (d) show those at 352 K. Each panel shows bare molecular ions as red symbols and complex ions as blue symbols. Fitting Eq. (5) to these data provides cross sections for each of the reaction channels and produces the solid lines in Fig. 2.

To isolate the energy-dependent reactivity from the steric effect, the ion yields are integrated over all angles, producing the curves shown in Fig. 3. The ratios $\frac{I(NeCO^+)}{I(CO^+)}$ and $\frac{I(NeN_2^+)}{I(N_2^+)}$ are shown in red and blue, respectively, over the entire energy range covered here, namely, between 0.2 K and 700 K. In the case of N_2, the formation of bare ions dominates over the entire energy range, while in the case of CO, the ratio becomes larger than one at energies below ≈100 K.

Inspection of the angle-dependent ratios permits to extract the steric effect in terms of total relative cross sections for $NeCO^+$ and CO^+ formation by quantifying the amplitude of the angle-dependent oscillations. The energy-dependent steric effect, as it is shown in Fig. 2(c) , is used to calculate the ratio between the relative ion yields at 180° and at 90°. This ratio, $r(\theta_{kB} = 180°)/r(\theta_{kB} = 90°)$, is a measure of the amplitude of the angle-dependent oscillations in bare ion vs complex formation. In Fig. 4, the plots for CO (red)

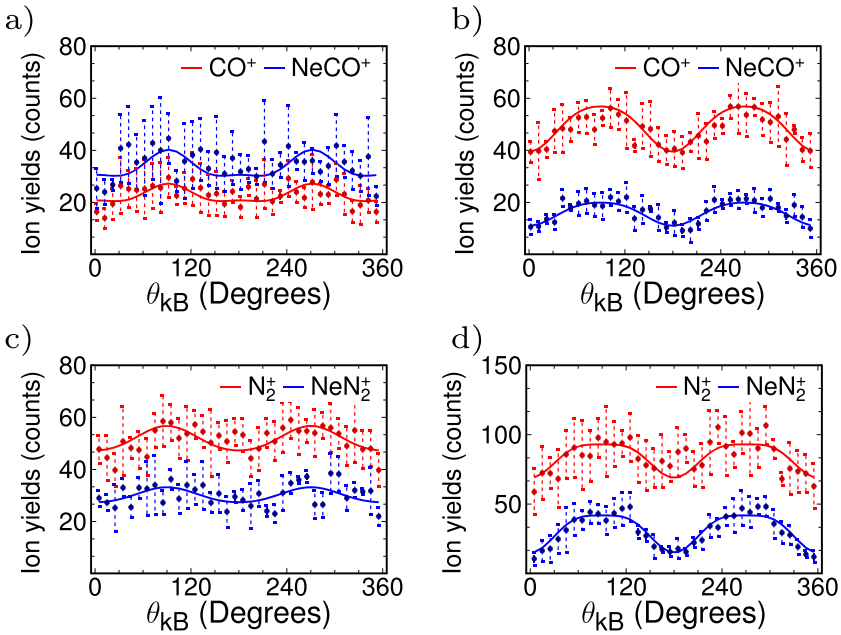

FIG. 2. Examples of angle-dependent ion yields: at E_{coll}/k_B = 600 mK for (a) the Ne* + CO collision and (c) the Ne* + N_2 collision and at E_{coll}/k_B = 352 K for (b) the Ne* + CO collision and (d) the Ne* + N_2 collision.

and N_2 (blue) can be seen, revealing a value of 1 at collision energies below ≈50 K for N_2 (blue symbols) and CO (red symbols), respectively, indicating that there is no orientation control at these energies. In contrast, at higher energies, the value is closer to 0.5, owing to the fact that $r(\theta_{kB})$ strongly fluctuates with the orientation angle. One may speculate that the steric effect in the case of CO disappears at higher energies already, but a definitive statement regarding this is not possible based on the present data. The same has also been observed in the case of Ne* reacting with Ar,[10] and it is attributed to a dynamic reorientation of the Ne* as it is approaching the secondary reactant at low speed.

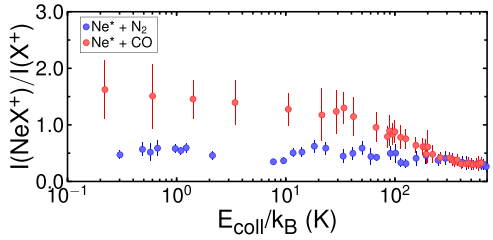

FIG. 3. Angle-integrated ratio of the Ne–X^+ and X^+ ion yields as a function of energy for X = CO (red) and X = N_2 (blue).

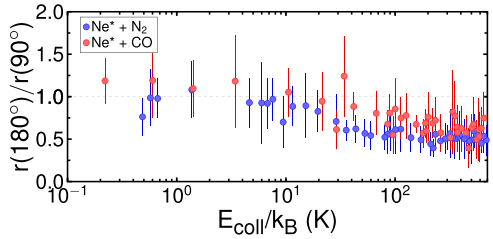

FIG. 4. The steric effect for N_2 (blue symbols) and CO (red symbols), defined as the ratio between the reactivities $r(\theta_{kB} = 180°)$ and $r(\theta_{kB} = 90°)$, as a function of energy. A value of 1 indicates no dependence of $r(\theta_{kB})$ on the Ne* orientation.

Our results from Ne* + Rg reactions show that the ion yield from PI does not depend on the orientation of Ne*.[9,48] In the case of the reactions with molecules, however, we also observe an angle-dependent yield of the bare ion, as seen in Fig. 2. For N_2, it was, furthermore, found that the observed relative yield of bare N_2^+ ions largely exceeded those from the rare gas reactions.[9] This was explained by invoking an additional reaction channel, namely, AI followed by predissociation (PD): in analogy with the rare gas reactions, it is assumed that PI is independent of the Ne* orientation, and the angle-dependent formation of bare ions is interpreted as being the result of predissociating AI complexes formed with vibrational excitation of the molecular fragment (see below). Predissociation takes place on a time scale faster than the extraction time of the ToF-MS; as a result, direct distinction between AI+PD and PI is not possible, only between $[Ne–CO]^+$ and CO^+.

To quantify the angle dependence in the red trace in Fig. 1(b), these dynamics are included in the analysis by using the following relationship between the observed X^+ signal and the true propensities for PI and AI, expressing the observed CO^+ ion yield as a linear combination of the PI yield and that of AI+PD:[9]

$$I_{X^+}(\theta_{kB}, E_{coll}) = w_{pd}(E_{coll}) I_{NeX^+}(\theta_{kB}, E_{coll}) + I_{PI}(E_{coll}), \quad (6)$$

where $w_{pd}(E_{coll})$ is the fraction of NeX^+ ions that predissociate, and $I_{PI}(E_{coll})$ is the direct yield of X^+ ions through PI. The predissociation probability then becomes $P_{pd} = \frac{w_{pd}}{1+w_{pd}}$.

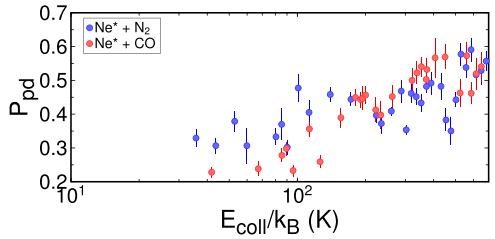

FIG. 5. Predissociation probability P_{pd} of the AI products $[Ne–X]^+$, obtained by fitting Eq. (6) to the experimental data, for X = CO (red) and X = N_2 (blue).

P_{pd} does not depend on the magnetic field direction, but can vary with collision energy. The actual ratio between AI and PI then becomes

$$\frac{I_{AI}}{I_{PI}} = \frac{I_{NeX^+}(\theta_{kB}) + w_{pd} I_{NeX^+}(\theta_{kB})}{I_{X^+}(\theta_{kB}) - w_{pd} I_{NeX^+}(\theta_{kB})}, \tag{7}$$

which defines the reactivity (explicit indication of the dependence of each term on the collision energy is omitted for clarity). This approximation only works at collision energies above ≈50 K because below that no steric effect is observed, and the reactivity becomes independent of θ_{kB}.

The same formalism is also used to analyze the CO data. The resulting probability for predissociation, P_{pd} is shown, together with the N_2–data, as a function of energy in Fig. 5, revealing the same upward trend with increasing energy for CO (red) and for N_2 (blue).

Finally, Fig. 6 shows the PD-corrected reactivities as a function of energy, after integration over all angles. These data show a similar trend as observed in Fig. 3, namely, the probability for AI and PI is nearly the same at all energies in the case of N_2, but the probability for AI is about two times higher than that for PI at low energies in the case of CO.

At first sight, the results from the Ne* + N_2 and Ne* + CO reactions appear very similar. There are, however, notable differences that are at the core of the following analysis. Inspection of the above data reveals the following:

1. For both reactions, the X^+ and $[Ne–X]^+$ signals are sensitive to the magnetic field direction. This is different from the observations for the analogous reactions between Ne* and ground state rare gas atoms.[10]

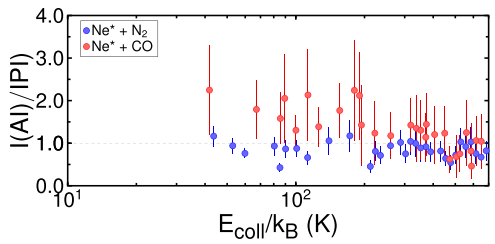

FIG. 6. Ratio of the angle-integrated AI and PI yields for N_2 (blue) and CO (red). In contrast to the data in Fig. 3, these data take into account predissociation using Eq. (7).

2. Loss of the orientation dependence is observed at collision energies below ≈50 K, possibly at slightly higher energies in the case of CO, similar to the rare-gas cases.
3. The N_2^+ yield dominates over the $[Ne–N_2]^+$ yield in the entire energy range; while in the case of CO, the formation of complex ions dominates at low energy.

The Ne($^3P_2$) + N_2 reaction has been compared with Ne* + Rg reactions previously, and it was found that predissociation of complexes with at least one quantum of vibrational excitation reduces the observed yield of complex ions, as it is also seen here in the case of CO. The binding energy of Ne(^1S)–N_2^+ is estimated to be 300 cm^{-1},[59] that of Ne(^1S)–CO^+ has been calculated to be 491 cm^{-1},[55] while the vibrational frequencies of the bare molecular ions are w_e = 2207 cm^{-1} and w_e = 2214.24 cm^{-1}, respectively.[56] Since it has been observed in the past that energy transfer from the metastable Ne* to molecules can lead to substantial vibrational excitation of the resulting ion,[54] it is reasonable to assume that also the associative ionization reaction leads to complexes with vibrationally excited molecular moieties, but these are not stable and predissociate by vibrational energy transfer from the molecular bond to the $[Ne–X]^+$ bond.

N_2 and CO are isoelectronic molecules with similar properties in many respects.[57] To understand the difference in the chemi-ionization, we turn to the vibronic structures of the two product ions CO^+ and N_2^+. Figure 7 shows the relevant energy levels for the case of CO. The ionization potential of CO is 14.014 eV, that of N_2 is 15.581 eV, corresponding to excess energies of 20 986.54 cm^{-1} and 8347 cm^{-1}, respectively, when these two molecules undergo PI with Ne($^3P_2$). In both cases, the complex's binding energy is lower than the vibrational frequency of the molecular ion and, hence, leaves the PD channel open for any complex ion that is not formed in the vibrational ground state. Because of the lower ionization energy, in the case of CO vibrational levels up to v^+ = 10 (at 133 202 cm^{-1}) are accessible, while in the case of N_2, the highest known accessible state has v = 3, while the energy of the Ne(^1S)–N_2^+(v = 4) state lies very close to the energy of the reactants, but the binding energy of the complex is not known with sufficient accuracy to tell with certainty whether or not it is energetically accessible in the present experiment.

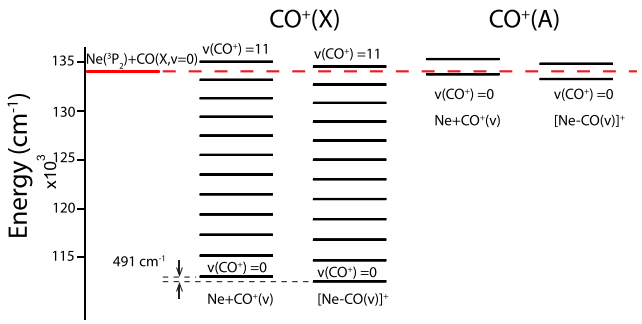

FIG. 7. Relevant energy levels for the Ne($^3P_2$) + CO reaction. Successive vibrational levels of CO are indicated in each case. For both accessible electronic states, the levels of the bare ion are shown on the left, and those of the complex are shown on the right.

The major difference between CO and N_2 is found in the electronic structure: the first excited state of N_2^+, the $A^2\Pi_{ui}$ state, lies 9166 cm^{-1} above the ground state of the ion, 134 826 cm^{-1} above the neutral ground state, and the energy of $Ne(^3P_2)$ being 133 880 cm^{-1}; this state is not accessible in this experiment even at the highest collision energies. In contrast, the first electronically excited state of CO is the $A^2\Pi_i$ at an energy of 20 733 cm^{-1} above the ionic ground state, 133 755 cm^{-1} above the ground state of neutral CO. As shown in Fig. 7, this opens two additional reaction channels, namely, AI and PI forming Ne–CO^+(A) and bare CO^+(A), respectively. Assuming that the $[Ne–CO]^+$ binding energy is similar for CO^+(X) and for CO^+(A), it is seen that in the case of the electronically excited CO^+, only the vibrational ground state is accessible, ruling out the possibility of vibrational PD after AI.

As a consequence, and unlike in the case of the rare gases or N_2, a detailed analysis of the reactivity in the case of CO must include the channels leading electronically excited ions. The present experiment at this time cannot distinguish between the formation of the two electronic states. However, by assuming that electronic predissociation, corresponding to the process Ne–CO^+(A, v = 0) → Ne + CO^+(X, v), is slow on the experimental time scale, the different observations of the AI/PI ratios in N_2 and CO can be explained by the fact that the AI products with electronically excited CO^+ do not predissociate at all, and by invoking a threshold dependence in the different cross sections leading to CO^+(A) and CO^+(X). These assumptions imply that in the range of collision energies below ≈200 K, the formation of electronically CO^+(A) and Ne–CO^+(A) gain in relative importance, and the absence of PD explains the overall increase in the relative contribution of AI.

However, this simplified model makes assumptions that demand further testing: (1) it is assumed that PI is independent of the Ne^* orientation, in analogy with the rare gases, and for both molecules studied here, independent of the final electronic state of the ion. Beyond the observations with the rare gases, the present experiment does not currently permit to test this assumption experimentally, and theoretical support is required. (2) Detection of only the final product ions does not permit the positive confirmation that CO^+(A) is formed. Penning ionization electron spectra are required for this, where the excited state would appear in the form of slow Penning electrons. According experiments are currently underway in our laboratory. (3) While not critical for the present analysis, the Penning electron spectra will rely on the time scale for electronic predissociation, which at present is not known. This aspect will have to be addressed both experimentally and theoretically.

IV. CONCLUSIONS

A merged beam study of the reaction between CO and oriented metastable Ne in a range of collision energies between 200 mK and 700 K is described, and the results are analyzed in comparison with previous results from the Ne^* + N_2 reaction. Three principal reaction pathways are observed: Penning ionization [yielding products $Ne(^1S)$ + CO^+], associative ionization (yielding Ne–CO^+ complexes), and associative ionization, followed by predissociation [also producing $Ne(^1S)$ + CO^+]. Their dependence on collision energy and the Ne^* orientation is studied by orienting Ne^* in a magnetic field and recording products using a mass spectrometer. In order to include the predissociation channel in the analysis, Penning ionization was assumed independent of the Ne^* orientation, in analogy with observations in reactions of Ne^* with rare gas atoms.

The main difference between the reactions with CO and those with N_2 is found in the increased probability of complex formation in the case of CO. While the detected ratio between CO^+ and Ne–CO^+ implicitly includes predissociation, this trend remains even when PD is accounted for. The difference between N_2 and CO is attributed to the fact that the lowest electronically excited state of CO^+, the A-state, lies within the range of accessible energies; while in the case of N_2, no electronically excited state can be reached. Because only the vibrational ground state of the CO^+(A) can be populated, this state increases the total cross section for complex formation.

It should be noted that even though one might expect a difference between N_2 and CO that could be attributed to the reduced symmetry in CO, no such effect could be found. The $^1\Sigma^+$ ground state of CO is only very slightly polar (dipole moment of 0.122 D[58]), explaining why the potential energy surface of Ne^*–N_2 and Ne^*–CO may be sufficiently similar to not lead to fundamentally different reactivities. Furthermore, several rotational states are populated in the molecule, producing an effectively apolar, isotropic object as seen by the approaching Ne^*. Nonetheless, extensive calculations of both systems are necessary to get a full understanding of the experimental observations.

ACKNOWLEDGMENTS

This project was funded by the Swiss Science Foundation (Grant Nos. 200021_165975 and 200020_184944). We thank our colleagues from Professor Mazzanti's group (EPFL) for lending us CO gas.

DATA AVAILABILITY

The data that support the findings of this study are available from the corresponding author upon reasonable request.

REFERENCES

[1] *Cold Chemistry; Molecular Scattering and Reactivity Near Absolute Zero*, edited by O. Dulieu and A. Osterwalder (Royal Society of Chemistry, Cambridge, 2017).
[2] R. V. Krems, Phys. Chem. Chem. Phys. **10**, 4079 (2008).
[3] N. Balakrishnan, J. Chem. Phys. **145**, 150901 (2016).
[4] B. K. Stuhl, M. T. Hummon, and J. Ye, Annu. Rev. Phys. Chem. **65**, 501 (2014).
[5] Z. Gao, T. Karman, S. N. Vogels, M. Besemer, A. van der Avoird, G. C. Groenenboom, and S. Y. T. van de Meerakker, Nat. Chem. **10**, 469 (2018).
[6] A. B. Henson, S. Gersten, Y. Shagam, J. Narevicius, and E. Narevicius, Science **338**, 234 (2012).
[7] E. Lavert-Ofir, Y. Shagam, A. B. Henson, S. Gersten, J. Kłos, P. S. Żuchowski, J. Narevicius, and E. Narevicius, Nat. Chem. **6**, 332 (2014).
[8] Y. Segev, M. Pitzer, M. Karpov, N. Akerman, J. Narevicius, and E. Narevicius, Nature **572**, 189 (2019).
[9] J. Zou, S. D. S. Gordon, and A. Osterwalder, Phys. Rev. Lett. **123**, 133401 (2019).
[10] S. D. S. Gordon, J. J. Omiste, J. Zou, S. Tanteri, P. Brumer, and A. Osterwalder, Nat. Chem. **43**, 7279 (2018).
[11] S. D. S. Gordon, J. Zou, S. Tanteri, J. Jankunas, and A. Osterwalder, Phys. Rev. Lett. **119**, 053001 (2017).

[12]L. R. Liu, J. D. Hood, Y. Yu, J. T. Zhang, N. R. Hutzler, T. Rosenband, and K.-K. Ni, Science **360**, 900 (2018).
[13]K.-K. Ni, S. Ospelkaus, D. Wang, G. Quéméner, B. Neyenhuis, M. H. G. De Miranda, J. L. Bohn, J. Ye, and D. S. Jin, Nature **464**, 1324 (2010).
[14]W. E. Perreault, N. Mukherjee, and R. N. Zare, Science **358**, 356 (2017).
[15]C. Amarasinghe and A. G. Suits, J. Phys. Chem. Lett. **8**, 5153 (2017).
[16]C. Amarasinghe, H. Li, C. A. Perera, M. Besemer, J. Zuo, C. Xie, A. van der Avoird, G. C. Groenenboom, H. Guo, J. Kłos *et al.*, Nat. Chem. **12**, 528 (2020).
[17]S. Y. T. van de Meerakker, H. L. Bethlem, N. Vanhaecke, and G. Meijer, Chem. Rev. **112**, 4828 (2012).
[18]B. C. Sawyer, B. K. Stuhl, D. Wang, M. Yeo, and J. Ye, Phys. Rev. Lett. **101**, 203203 (2008).
[19]S. A. Rangwala, T. Junglen, T. Rieger, P. W. H. Pinkse, and G. Rempe, Phys. Rev. A **67**, 043406 (2003).
[20]B. Bertsche and A. Osterwalder, Phys. Chem. Chem. Phys. **13**, 18954 (2011).
[21]T. de Jongh, M. Besemer, Q. Shuai, T. Karman, A. van der Avoird, G. C. Groenenboom, and S. Y. T. van de Meerakker, Science **368**, 626 (2020).
[22]V. Plomp, Z. Gao, T. Cremers, M. Besemer, and S. Y. T. van de Meerakker, J. Chem. Phys. **152**, 091103 (2020).
[23]A. Bergeat, J. Onvlee, C. Naulin, A. Van Der Avoird, and M. Costes, Nat. Chem. **7**, 349 (2015).
[24]X. Wu, T. Gantner, M. Koller, M. Zeppenfeld, S. Chervenkov, and G. Rempe, Science **358**, 645 (2017).
[25]A. Osterwalder, EPJ Tech. Instrum. **2**, 10 (2015).
[26]J. Jankunas, B. Bertsche, K. Jachymski, M. Hapka, and A. Osterwalder, J. Chem. Phys. **140**, 244302 (2014).
[27]B. Bertsche, J. Jankunas, and A. Osterwalder, Chimia **68**, 256 (2014).
[28]B. Nichols, H. Chadwick, S. D. S. Gordon, C. J. Eyles, B. Hornung, M. Brouard, M. H. Alexander, F. J. Aoiz, A. Gijsbertsen, and S. Stolte, Chem. Sci. **6**, 2202 (2015).
[29]H. Pan, F. Wang, G. Czakó, and K. Liu, Nat. Chem. **9**, 1175 (2017).
[30]F. Wang, K. Liu, and T. P. Rakitzis, Nat. Chem. **4**, 636 (2012).
[31]F. Wang, J.-S. Lin, and K. Liu, Science **331**, 900 (2011).
[32]H. Ohoyama, K. Yasuda, and T. Kasai, J. Phys. Chem. A **112**, 10716 (2008).
[33]D. Watanabe, H. Ohoyama, T. Matsumura, and T. Kasai, J. Chem. Phys. **125**, 224301 (2006).
[34]M. H. G. De Miranda, A. Chotia, B. Neyenhuis, D. Wang, G. Quéméner, S. Ospelkaus, J. L. Bohn, J. Ye, and D. S. Jin, Nat. Phys. **7**, 502 (2011).
[35]S. D. S. Gordon and A. Osterwalder, Annu. Rev. Phys. Chem. **39**, 109 (2020).
[36]J. J. Omiste, J. Floß, and P. Brumer, Phys. Rev. Lett. **121**, 163405 (2018).
[37]P. E. Siska, Rev. Mod. Phys. **65**, 337 (1993).
[38]M. B. Arfa, B. Lescop, M. Cherid, B. Brunetti, P. Candori, D. Malfatti, S. Falcinelli, and F. Vecchiocattivi, Chem. Phys. Lett. **308**, 71 (1999).
[39]F. Biondini, B. G. Brunetti, P. Candori, F. De Angelis, S. Falcinelli, F. Tarantelli, M. Moix Teixidor, F. Pirani, and F. Vecchiocattivi, J. Chem. Phys. **122**, 164307 (2005).
[40]B. Brunetti, P. Candori, D. Cappelletti, S. Falcinelli, F. Pirani, D. Stranges, and F. Vecchiocattivi, Chem. Phys. Lett. **539-540**, 19 (2012).
[41]S. Falcinelli, F. Vecchiocattivi, and F. Pirani, Commun. Chem. **3**, 64 (2020).
[42]S. Falcinelli, F. Vecchiocattivi, and F. Pirani, J. Chem. Phys. **150**, 044305 (2019).
[43]S. Falcinelli, F. Pirani, P. Candori, B. G. Brunetti, J. M. Farrar, and F. Vecchiocattivi, Front. Chem. **7**, 445 (2019).
[44]J. Jankunas, K. S. Reisyan, T. P. Rakitzis, and A. Osterwalder, Mol. Phys. **114**, 245 (2016).
[45]R. N. Zare, *Angular Momentum: Understanding Spatial Aspects in Chemistry and Physics* (Wiley-Interscience, New York, 1988).
[46]T. P. Rakitzis and R. N. Zare, J. Chem. Phys. **110**, 3341 (1999).
[47]A. J. Orr-Ewing and R. N. Zare, Annu. Rev. Phys. Chem. **45**, 315 (1994).
[48]S. D. S. Gordon and A. Osterwalder, Phys. Chem. Chem. Phys. **21**, 14306 (2019).
[49]D. Bellert and W. H. Breckenridge, Chem. Rev. **102**, 1595 (2002).
[50]J. A. Beswick, N. Halberstadt, and K. C. Janda, Chem. Phys. **399**, 4 (2012).
[51]J. Zou, S. D. S. Gordon, S. Tanteri, and A. Osterwalder, J. Chem. Phys. **148**, 164310 (2018).
[52]K. Luria, N. Lavie, and U. Even, Rev. Sci. Instrum. **80**, 104102 (2009).
[53]J. Jankunas, B. Bertsche, and A. Osterwalder, J. Phys. Chem. A **118**, 3875 (2014).
[54]D. M. Sonnenfroh and S. R. Leone, Int. J. Mass Spectrom. Ion Processes **80**, 63 (1987).
[55]R. Kong, X. Shan, S. Wang, Y. Zhang, L. Sheng, L. Hao, and Z. Wang, J. Electron Spectrosc. Relat. Phenom. **160**, 49 (2007).
[56]P. J. Linstrom and W. G. Mallard, J. Chem. Eng. **46**, 1059 (2001).
[57]H. Hotop and A. Niehaus, Int. J. Mass Spectrom. **5**, 415 (1970).
[58]G. E. Scuseria, M. D. Miller, F. Jensen, and J. Geertsen, J. Chem. Phys. **94**, 6660 (1991).
[59]E. J. Bieske, A. M. Soliva, and J. P. Maier, J. Chem. Phys. **94**, 4749 (1991).